Nanoperiodic Arrangement of Crystal/Amorphous Phases Induced by Tensile Drawing of Highly Entangled Polyethylene

Hiroki Uehara,* Kei-ichi Takeuchi, Masaki Kakiage, Takeshi Yamanobe, and Tadashi Komoto

Department of Chemistry, Gunma University, Kiryu, Gunma 376-8515, Japan

Received April 19, 2007; Revised Manuscript Received May 21, 2007

ABSTRACT: A nanoperiodic crystalline/amorphous arrangement was homogeneously developed by tensile drawing and subsequent annealing of ultrahigh molecular weight polyethylene (UHMW-PE) lamellae, trapping a large number of molecular entanglements on their surfaces. Lozenge crystalline blocks 40 nm in edge appeared regularly packed, producing the meshlike amorphous channels 5 nm wide. A grid-rotation analysis based on transmission electron microscopy observations indicated characteristic bicontinuous arrangements of crystalline and amorphous phases. The results of the small-angle X-ray scattering measurements for the drawn sample also supported this unique phase packing model.

Introduction

Recently, the nanoperiodic structure of the polymeric materials has elicited a great deal of interest for preparing nanoporous films or membranes.[1−14] The most popular approach involves utilizing the block copolymers, which produce the self-assembled phase separation induced by the different segments.[8] Nanoporous structure can be produced when one of the segmental phases within the obtained phase separation is etched by various chemical treatments[1−8,12] or foamed by the supercritical fluids.[9−11,13] We successfully prepared a nanoporous polyethylene (PE) membrane from a block copolymer precursor.[15] The excellent flexibility obtained is preferable for various applications, including separation membranes or substrates for cell multiplication. The superior property of the resultant nanoporous structure is ascribed to the continuous morphology of the residual PE backbones, which has the simplest molecular architecture but produces a highly crystalline state.

Even pure semicrystalline polymers produce the nanometer-sized phase separation composed of crystalline and amorphous components. However, their nanoperiodic assembly has not been attempted, despite the wide usage and high processing ability that are the typical advantages of conventional semicrystalline polymers like PE. Usual melt crystallization of normal molecular weight PE (NMW-PE) produces the micrometer-sized spherulites containing crystalline and amorphous phases appearing in a radial orientation from the center (Figure 1a). The thickness of this lamellar morphology is controllable by the crystallization temperature.

In contrast, the ultrahigh-molecular-weight polyethylene (UHMW-PE), having long chains of over 10^6 MW, produces an ambiguous spherulite structure for crystallization from the melts (Figure 1b). Their lamellar thickness is constant at 30 nm,[16] independent of melt-crystallization conditions. It should be noted that this lamellar thickness value corresponds to the length of a straight chain segment with an MW of 1.7×10^3, which is the same as the critical MW between entanglements in PE melts.[17] This coincidence implies that the molecular entanglements contained in the prior melt are trapped on the lamellar surface during crystallization. Rastogi et al.[18,19] reported that the longer reparation time of UHMW chains prevents the disentanglement during crystallization. Therefore, we considered that they could play a role similar to that of segmental linkages located on the phase boundary for block copolymers.

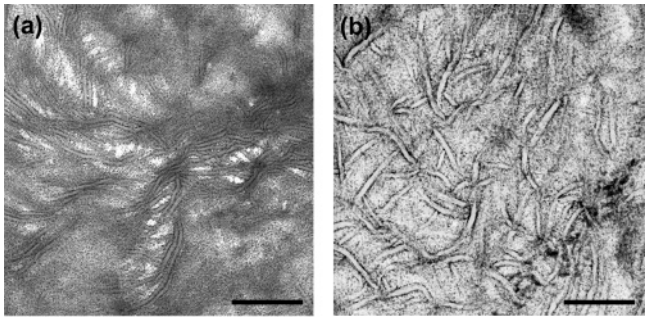

Figure 1. Comparison of TEM images for the initial spherulite structure of the melt-crystallized PE prepared in this study: (a) $M_w = 7.1 \times 10^4$ (NMW-PE1); (b) $M_w = 1.1 \times 10^6$ (UHMW-PE). Scale bar: 300 nm.

Deformation for the lamellar structure of block copolymers can vary the morphology into kink bands[20−24] or chevron patterns.[25,26] The effective stress transmission within both softer and harder components through the segmental linkages results in homogeneous deformation within the whole sample area. Such a combination of separated phases, with different properties yet connected to each other by segmental linkages, is similar to that of the crystalline and amorphous layers tied each other by the entanglements trapped on UHMW-PE lamellar surfaces. For these reasons, we chose UHMW-PE as a model material for nanometer assembling of semicrystalline polymer.

Experimental Section

Materials. The UHMW-PE used in this study was Hizex 240M supplied from Mitsui Chemical. Its molecular characteristics were analyzed by gel permeation chromatography (GPC) in a solvent of 1,2,4-trichlorobenzene at Tosoh (Yokkaichi, Japan) using standard methods. Weight- and number-average MWs are listed in Table 1. For comparison, two NMW-PEs with different MW distributions were used to estimate the effect of the lower MW components on tensile-deformed morphology.

Sample Preparation. The initial 150 μm thick film was prepared by casting from hot *p*-xylene solution with 1 wt % of PE material.

* Corresponding author. E-mail: uehara@chem-bio.gunma-u.ac.jp.

10.1021/ma070915z CCC: $37.00
Published on Web 07/10/2007

Table 1. Molecular Weights of the PE Materials Used in This Study

sample	$10^{-4}M_n$	$10^{-4}M_w$	M_w/M_n
UHMW-PE	11	110	10
NWM-PE1	1.7	7.1	4.1
NMW-PE2	3.9	11	2.8

This procedure erased the powder boundary of as-received materials, resulting in a homogeneous state in the resultant film. Such cast films were melt-annealed at 180 °C for 20 min in a vacuum, followed by slow cooling to room temperature. The obtained sample films were cut into strips 30 mm long and 5 mm wide and tensile-drawn in an air oven equipped with a Tensilon RTM-1425 tensile tester. Draws were performed at constant temperatures (T_d) from room temperature to 120 °C and at cross-head speeds corresponding to an initial strain rate of 1 min^{-1}. Before drawing, each sample was kept in an oven at a given T_d for 5 min. After drawing, subsequent annealing was performed for 24 h at a temperature (T_a) of 80−120 °C with the sample ends fixed. The draw ratio (*DR*) was determined from the separation of ink marks preprinted on the surface of the samples.

Structural Analyses. The drawn morphology was analyzed by transmission electron microscopy (TEM) observations using a JEOL 1200EX electron microscope operated at 80 kV. The samples were stained with RuO_4 vapor and embedded in epoxy resin. RuO_4 vapor selectively stained the amorphous regions; thus, those regions appeared darker than the crystalline regions in the TEM images in this study. The assembly was cut into thin sections 50 nm thick using a Reichert UltraCut S microtome. Grid rotation analysis was applied for modeling the crystalline and amorphous packing within the sample. The Fourier transformation of the TEM image was also performed using a free-software ImageJ (http://rsb.info.nih.gov/ij/).

Small-angle X-ray scattering (SAXS) measurements were carried out by using a synchrotron radiation source at the BL40B2 beamline of SPring-8 (Japan Synchrotron Radiation Research Institute, Hyogo, Japan). The SAXS patterns of the drawn film were recorded on a cooling-type CCD camera (Hamamatsu Photonics, C4880) with an image intensifier (Hamamatsu Photonics, V5455P). The wavelength of the synchrotron beam was 1.54 Å, camera length was 1.96 m, and background scattering was subtracted from the series of the observed patterns.

Results and Discussion

Typical Morphologies of Deformed PE. Tensile drawing of the melt-crystallized lamellae of NMW-PE results in a mixture of lamellar inclination and fragmentation, depending on the position within the spherulite.[27] Figure 2 depicts the typical drawn morphology of the melt-crystallized NMW-PE. A wavy lamellar structure is observed with an ambiguous periodicity of the crystalline and amorphous phases.[28,29]

In contrast, our UHMW-PE material took on a characteristic nanoperiodic morphology that was quite different from those of NMW-PEs. A typical TEM image of the drawn UHMW-PE is presented in Figure 3. The film was tensile-drawn up to a draw ratio (*DR*) of 4 at 80 °C and subsequently annealed at 120 °C with the film ends fixed for 24 h. The obtained image revealed bright lozenge crystalline blocks 40 nm in edge length periodically arranged diagonally along the draw direction and were divided by a dark amorphous mesh 5 nm wide. A similar rectangular bricklike image has been obtained for TEM observation of the triblock copolymer system, giving various self-assembled phase arrangements depending on the balance of the segmental lengthes.[30] These facts imply that the trapped entanglement on UHMW-PE lamellar surface are comparable to the segmental linkages located on the phase boundary for block copolymers.

Another characteristic of our nanoperiodic morphology homogeneously is its spreading within the wider spatial area

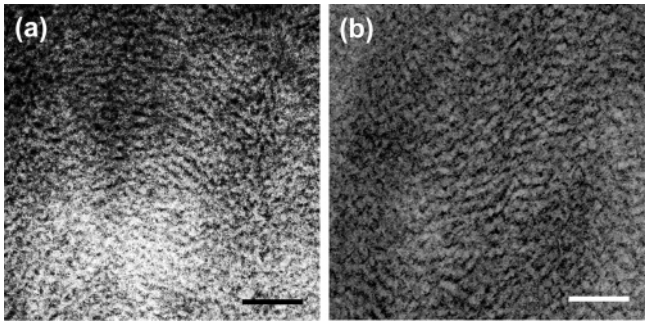

Figure 2. Tensile-drawn morphologies of the melt-crystallized NMW-PE films: (a) $M_w = 7.1 \times 10^4$ (NMW-PE1); (b) $M_w = 11 \times 10^4$ (NMW-PE2). Scale bar: 100 nm. Tensile drawing was performed at 80 °C up to the same *DR* of 7.0. The draw direction was vertical.

over several tens of micrometers. Similar images were obtained for different positions of the sample, indicating that such periodic arrangements of crystalline and amorphous phases were spread over a centimeter scale. In these TEM images, the amorphous layer appeared continuous with a meshlike arrangement; however, the crystalline blocks looked separated from each other. Detailed arrangements of these crystalline and amorphous phases will be discussed later with the possible structural packing model.

The spatial periodicity of these crystalline and amorphous arrangements could be confirmed by the Fourier transformation procedure.[24] The inset image in Figure 3 was obtained by such transformation for the whole area of this TEM image. The result exhibited a typical four-point pattern quite similar to that of SAXS for the deformed block copolymers initially providing the lamellar morphology.[21−23,26,31,32] However, the tensile-drawn NMW-PE usually exhibits a symmetrical set of two-line scattering on the SAXS pattern, which separates perpendicularly to the draw direction.[33−35] Therefore, the four-point Fourier transformation pattern, reflecting the periodic arrangements of the lozenge crystalline blocks and meshlike amorphous channels, was characteristic for the tensile-drawn UHMW-PE.

Even for UHMW-PE, a two-line SAXS pattern was obtained when the sample film was crystallized from the solution.[36] The regular stacking of the single-crystal lamellae results in a 10 nm periodicity,[36,37] which was much smaller than that for the melt-crystallized UHMW-PE lamellae prepared in this study. Annealing of these solution-crystallized lamellae induces the so-called thickness "doubling" phenomenon[38] due to chain slippage along the normal lamellar normal direction. Higher molecular mobility is accelerated by the less entangled state of the solution-crystallized lamellae.[16,36] Correspondingly, this structure is ultradrawable into extended chain crystals (ECCs) by tensile drawing up to the highest *DR* of a hundred or more.[39,40] In contrast, simple annealing of the melt-crystallized UHMW-PE yielded no structural reorganization,[16] which was prevented by the trapped entanglements on the lamellar surface.

Effects of Preparation Conditions on Deformed Morphology. Optimum sets of the drawing and annealing conditions exist for preparing such typical nanoperiodic arrangements of crystalline and amorphous phases. First, the effects of drawing conditions on the resultant morphologies were examined. Figure 4 compares TEM images of the melt-crystallized UHWM-PE film drawn at different T_ds ranging from room temperature to 120 °C. The maximum *DR* increased from 2.4 to 9.0 with increasing T_d. Therefore, the comparable *DR* of 4 could be achieved at a T_a range from 60 to 120 °C, but the lower *DR* of 2.4 at room temperature was adopted for comparison in Figure

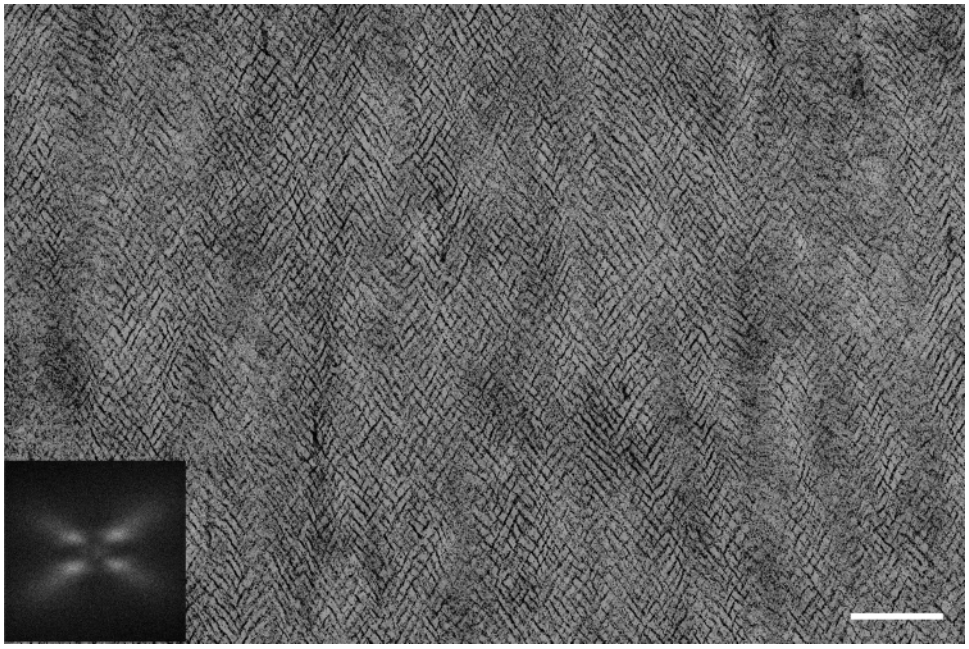

Figure 3. Typical TEM image of nanoperiodic crystal/amorphous phase arrangement for drawn UHMW-PE film within the wider spatial area. The draw was made at 80 °C up to a *DR* of 4.0, and the sample was subsequently annealed at 120 °C with film ends fixed. Scale bar: 300 nm. The draw direction was vertical. The inset is a Fourier-transformed image.

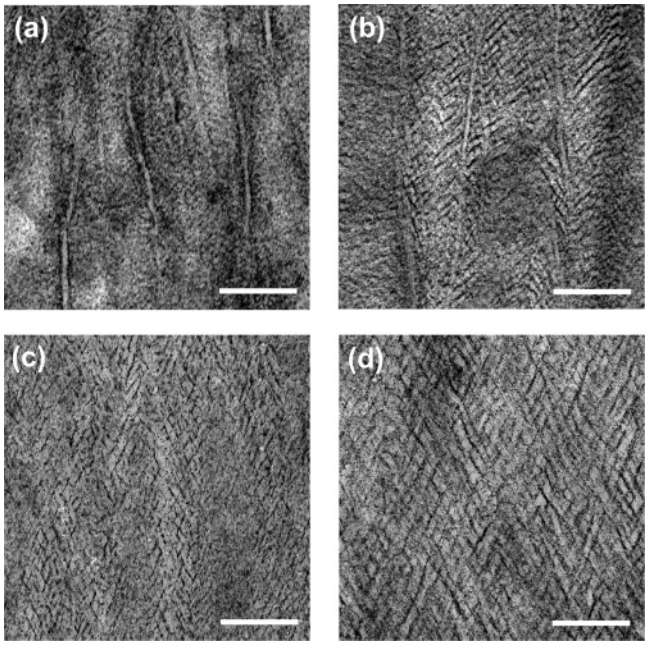

Figure 4. TEM images for the UHMW-PE film drawn at various T_d's: (a) T_d = room temperature, $DR = 2.4$; (b) $T_d = 60$ °C, $DR = 4.0$; (c) $T_d = 80$ °C, $DR = 3.8$; (d) $T_d = 120$ °C, $DR = 4.1$. Scale bar: 200 nm. The draw direction was vertical.

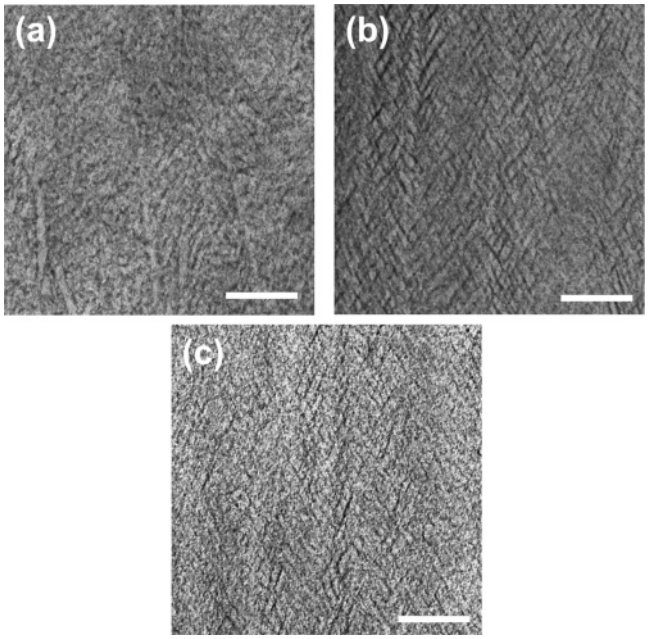

Figure 5. Changes in drawn morphologies of the UHMW-PE films with increasing *DR* at a T_d of 80 °C: (a) $DR = 2.8$, (b) $DR = 4.8$, and (c) $DR = 5.3$. Scale bar: 150 nm. The draw direction was vertical.

4. Even at such a comparable *DR*, the drawn morphologies varied depending on T_d. At the lower T_d of 60 °C (b), straight lamellae were observed with an orientation parallel to the draw direction. Such straight lamellae looked just inclined along the drawing direction (i.e., the surviving morphology of the prior lamellae). The number of these surviving lamellae was larger for drawing at room temperature (a). In contrast, straight lamellae were not obsereved for the higher T_d over 80 °C (c). Instead, the targeted nanoperiodic structure homogeneously spread within the wider spatial area over 1 mm. However, the size of the lozenge crystalline blocks increased with increasing T_d. The resultant lamellar thickness increases with increasing T_d for NMW-PE,[41] indicating that deformation-induced crystallization in this T_d range was accompanied by mechanical melting of the initial lamellae. The higher T_d of 150 °C produced a so-called shish-kebab morphology composed of a combination of ECCs and folded-chain crystals (FCCs).[42] We[43−45] previously found that tensile drawing of UHMW-PE in the molten state results in such a shish-kebab morphology. Thus, the drawing at a T_d of 150 °C was categorized as melt-drawing.

Even at the same T_d, *DR* was another important factor for the development of the targeted nanoperiodic structure. Figure 5 depicts the morphological changes upon drawing at a T_d of 80 °C, which gave the most periodic phase arrangements in Figure 4. The straight lamellae are survived at the lower *DR* of 2.8, but the characteristic combination of lozenge crystalline blocks and meshlike amorphous channel was obtained for a

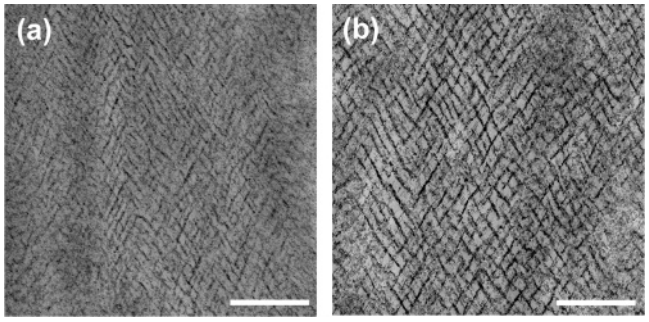

Figure 6. Influence of annealing on the tensile-drawn morphology of the UHMW-PE film: (a) T_a = 80 °C; (b) T_a = 120 °C. Annealing with ends fixed was performed for 24 h. Scale bar: 200 nm. The draw direction was vertical.

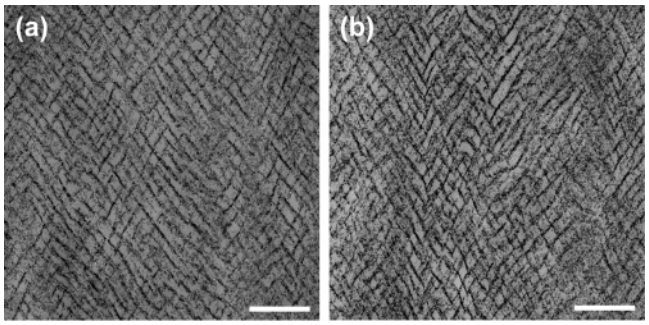

Figure 7. Comparison of the through-viewed and edge-viewed TEM images with comparable magnification. The sample is the same as in Figure 3. Scale bar: 150 nm. The draw direction was vertical.

higher *DR* of 4.8. However, the periodicity of such characteristic phase arrangements was lacking at the higher *DR* of 5.3. This result indicated that the preparation of targeted nanoperiodic morphology required an optimum *DR*, which was lower than the maximum achievable *DR*. Generally, the latter *DR* gives the highest mechanical properties along the drawing direction, corresponding to the highest molecular orientation.

Sample shrinkage is another possible cause of this characteristic nanoperiodic morphology. The sample drawn under an optimum T_d of 80 °C up to a *DR* of 4 exhibited the shrinkage of 20% of its length, producing the compression force applied to the drawn morphology. Such sample shrinkage could be reduced by annealing when the sample length was maintained in a Tensilon chamber after drawing. Figure 6 compares the TEM images obtained after annealing at 80 and 120 °C for 24 h. The sample film was initially tensile-drawn at 80 °C up to a *DR* of 4. Annealing at the higher T_a of 120 °C emphasized the boundaries between the crystalline blocks and amorphous mesh. Correspondingly, sample shrinkage was reduced from 13% for a T_a of 80 °C to 2% for a T_a of 120 °C. These results indicated that sample shrinkage somewhat disorganized the nanoperiodic phase arrangement of the drawn morphology.

This characteristic nanoperiodic morphology spread along both directions through the sample thickness direction as well as parallel to the film surface. The thin sections for the TEM observation were microtomed parallel to the film surface (Figure 7a), so the observation direction was a through-view perpendicular to the film surface. Interestingly, an edge-viewed image of a thin section microtomed parallel to the film edge (Figure 7b) exhibited similar morphologies composed of diagonal arrangements of lozenge crystalline blocks and an amorphous mesh in the draw direction. These results revealed that the same morphology was spread across the film thickness on the micrometer scale. Such homogeneity of crystalline/amorphous phase arrangement with wider scales was characteristic of our

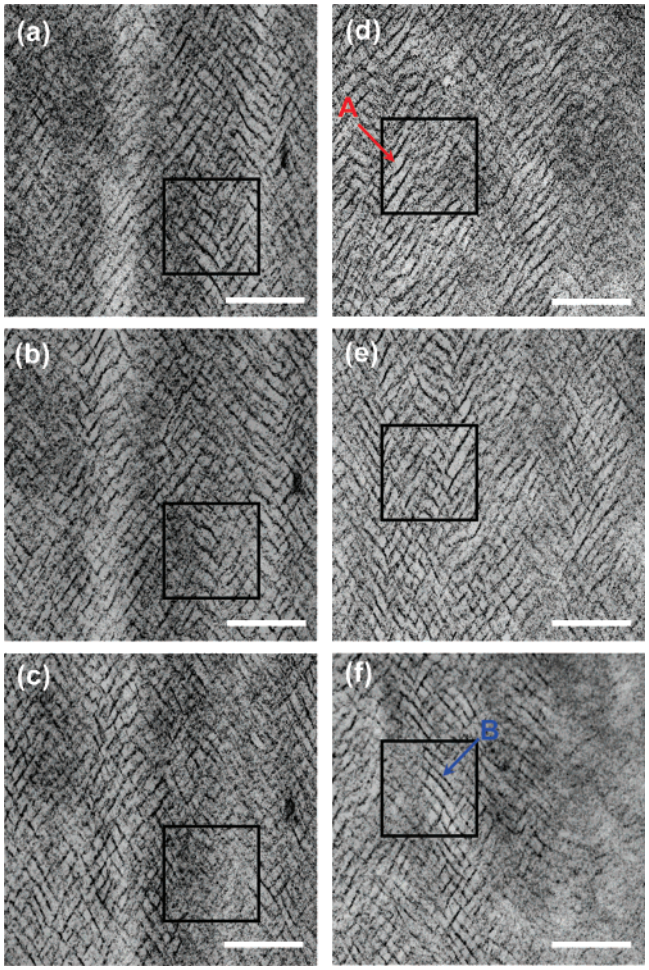

Figure 8. Tilt sets of through-viewed TEM images for drawn UHMW-PE: (a, d) −30°, (b, e) 0°, and (c, f) +30° tilted perpendicular (left) and parallel (right) to the draw direction. The sample is the same as in Figure 3. The draw direction was vertical. Amorphous layers with pairs of symmetric tilting angles are indicated by red arrow A and blue arrow B. Scale bar: 200 nm.

nanoperiodic morphology, prepared from PE composed by the simplest unit propagation but with UHMW introducing a larger amount of chain entanglements.

The periodicity of the crystalline/amorphous phase arrangement was less developed when the sample film was prepared by the usual compression molding of as-received UHMW-PE powder. This result was ascribed to residual powder boundaries on a micrometer scale remained due to the high melt viscosity of UHMW-PE. Our recent study[46] revealed that residual boundaries contained after film processing with UHMW-PE reactor powder cause heterogeneous stress transmission in the later ultradrawing process, resulting in inferior film properties reflecting the void formation within the sample film.

Phase Arrangement within Nanoperiodic Morphology. Such homogeneous spread of nanoperiodic pattern causes us an interest for possible arrangement of the crystalline and amorphous phases. To clarify the orientation of the lozenge crystalline blocks and amorphous meshes, grid-rotation analyses were employed on both the through and edge views. These rotations were set perpendicular and parallel to the draw direction in a TEM chamber. Figure 8 compares the sets of through-viewed images observed with the grid tilted from the normal plane to the indicated angles. The examined sample was tensile-drawn up to a *DR* of 4 at 80 °C and subsequently annealed at 120 °C with the film ends fixed for 24 h, which

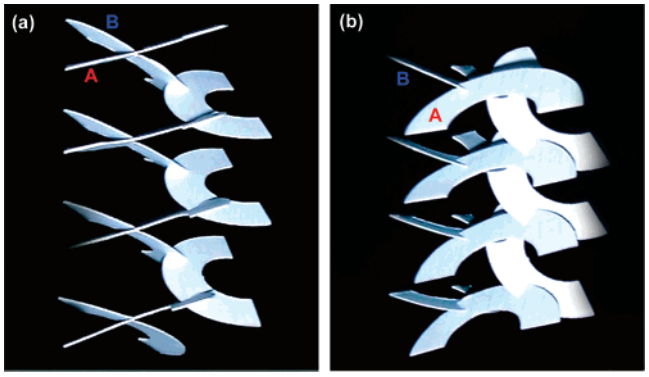

Figure 9. Schematic representation of continuous arrangement of amorphous layers: (a) through-viewed perpendicular to the draw direction (0° tilt); (b) +30° tilted parallel to the draw direction. Two symmetrically tilted amorphous layers are indicated by A and B, corresponding to layers A and B in Figure 8. The draw direction was vertical.

gave the most ordered nanoperiodic pattern (Figure 3). In the left column of Figure 8, the grid was tilted perpendicular to the draw direction. Both −30° (a) and +30° tilting (c) exhibited the typical features of the lozenge arrangement of crystalline blocks, similar to those observed under the nontilted condition (b). However, when the morphologies within a given position, surrounded by the solid square, were compared, the lozenge appearance was emphasized in Figure 8a but appeared unclear in Figure 8c. Similar results were obtained for the corresponding edge-viewed series of grid rotations perpendicular to the draw direction.

In contrast, the parallel rotation of a grid toward the draw direction resulted in a different appearance of the lozenge crystalline blocks. Figure 8d−f presents a series of images observed with the grid top tilted every 30° parallel to the draw direction. Two orientations of amorphous layers were clearly recognizable in these images. The right-up orientation of amorphous layers (A) was emphasized in Figure 8d, and the right-down orientation (B) was pronounced in Figure 8f; but both orientations appeared in Figure 8e. These results indicated that the alternate half of the diagonal inclination of the meshlike amorphous channel gradually disappeared with increasing rotation angle. These pairs of anisotropically emphasized amorphous layers reached across several crystalline blocks, suggesting lamellar-like packing of the amorphous phases. At the same time, these tilting procedures revealed the continuity of crystalline phases as well as that of amorphous layers. Namely, the crystalline regions were nominally divided by amorphous layers having different tilting angles toward the draw direction, resulting in the characteristic appearance of lozenge crystalline blocks in TEM images observed under a nontilted condition (Figure 8e). The homogeneous spread of this lozenge pattern in both through- and edge-viewed images means the long-range bicontinuity of the crystalline and amorphous layers within the whole sample bulk.

Focusing on the amorphous continuity developed within the sample internals enabled us to model the three-dimensional packing for this unique phase arrangement (Figure 9). The basis for this packing model was as follows. In order to maintain the periodicity of the lozenge crystalline packing in a series of TEM observation, the amorphous layer should tilt with a pair of symmetrical angles toward the draw direction within the whole region of the sample. If the width of these amorphous layers exceeded the microtomed thickness of 50 nm, amorphous layer stacking in either the right-up or the right-down direction would be emphasized. This result was inconsistent with the experimental result that both stacking directions of amorphous layers were observable in both through-viewed and edge-viewed images. Therefore, amorphous layers with two symmetrical inclinations must coexist. These inclinations of the amorphous layers (denoted with a red A and blue B in the figures) corresponded to those in Figure 8. However, only one of the inclined layer sets (B) was observable when this packing model was tilted to the front side (Figure 9b). This coincided well with the results in Figure 8d−f, where the grid was rotated parallel to the draw direction. It also supported the validity of the phase arrangement model proposed in Figure 9.

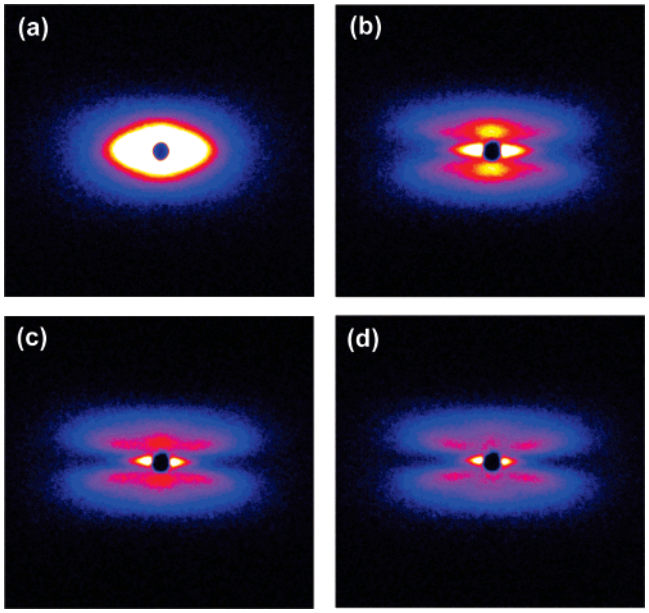

Figure 10. Series of through-viewed SAXS patterns recorded for the UHMW-PE films drawn at a T_d of 80 °C with different *DR*s: (a) *DR* = 2.0, (b) *DR* = 3.0, (c) *DR* = 4.0, and (d) *DR* = 5.0. The draw direction was vertical. The incident X-ray beam was radiated perpendicular to the film surface. Color gradation indicates scattering intensity.

Another feature of this phase arrangement model was the helical arrangement of the amorphous layers, which was required to satisfy the requirement that all viewing directions perpendicular to the draw direction give constant periodicity and symmetrical inclinations of the amorphous layers. Such a helical arrangement of the amorphous layers always gave two symmetrical inclinations when the TEM observations were made perpendicular to the draw direction (Figure 8a−c).

These helical ribbons of amorphous layers should be arranged in parallel and combine with each other to provide lateral continuity of the amorphous layers. If ECCs were placed in the core of these helical ribbons, the resulting combination of crystalline phases would be consistent with the so-called shish-kebab structure.[42] Odell et al.[47] proposed a structural model in which neighboring shish-kebab rows gear each other for oriented crystallization of NMW-PE induced by high-pressure extrusion. The difference between their model and ours lies in the focusing phase (i.e., the crystalline or amorphous arrangement). Our model emphasizes the continuity and the homogeneity of the amorphous phases, taking into account the larger number of molecular entanglements of the UHMW-PE chains, which act as linkages between crystalline and amorphous phases.

Such characteristic packing of crystalline and amorphous phases was also confirmed by SAXS measurements. Figure 10 depicts the changes in SAXS patterns during drawing at 80 °C for our UHMW-PE film. The initial isotropic pattern became horizontally elongated at a lower *DR* of 2, indicating the lamellae

inclination along the draw direction. This result was coincident with the TEM results presented in Figure 5. However, the patterns at the higher *DR* contained the different types of scatterings. At a *DR* of 3, a streak around the center and a vertical set of scattering halos were observed. Both the streak and the halos elongated perpendicular to the draw direction. A similar streak was been reported for ECCs of shish-kebab morphology for shear-crystallized PE.[48−50] In contrast, a vertical set of elongated halos exhibited the scattering maxima on the meridian, indicating that the normal lamellar stacking is distributed with a certain angle toward the draw direction. With further *DR* increasing up to 4, where the most desirable nanoperiodic arrangement of the crystalline and amorphous phases was obtained in TEM observation, the pattern exhibited four-point maxima on both edges of the top and bottom halos. However, other maxima still on the meridian were observed at the lower *DR*. Such scattering maxima on the meridian disappeared for the highest *DR* of 5. Here, it should be noted that the four-point pattern alone was obtained for the Fourier transformation of the targeted nanoperiodic morphology (Figure 3), reflecting the periodicities of the set of the diagonal arrangement of amorphous layers with a symmetrical inclination. In contrast, the additional meridian maxima in the SAXS pattern at the optimum *DR* of 4 were ascribed to the periodicity obtained at the linking regions of the helical amorphous layers in Figure 9. The crossing positions of helical amorphous layers A and B were periodically arranged parallel to the draw direction. The inclinations of the amorphous layers offset each other at these crossing regions; thus, the corresponding periodicity of the amorphous stacking resulted in less inclined maxima on the meridian. In other words, this coexistence of the meridian and four-point maxima was evidence that the crossing of the amorphous layers had symmetrical inclinations toward the draw direction. The disappearance of such meridian maxima for a *DR* of 5 also suggested the disarrangement of these connecting regions induced by structural breaking. This result was coincident with the TEM image in which the periodicity of the phase arrangement was disordered (Figure 5c). The scattering streaks near the center corresponded to the ECCs[48−50] that ran through the coils of the helical amorphous layers (Figure 9).

Bicontinuity of the crystal/amorphous phases was obtained for the block copolymer in our recent study.[15] Selective removal of the amorphous phase resulted in a nanoporous PE membrane with excellent flexibility. A similar porous material may be expected if correspondingly deep etching is applied to the bicontinuous crystal/amorphous arrays prepared in this study.

Conclusion

Highly uniform arrangements of the crystalline and amorphous phases were induced by tensile drawing of the highly entangled UHMW-PE. A combination of TEM and SAXS analyses enabled us to propose the bicontinuous packing of these phases spread within the wide spatial range of the sample. In contrast, the NMW-PE exhibited the ambiguous periodicity of the crystalline and amorphous components. The entanglement trapping on the lamellar surface of UHMW-PE was crucial for the preparation of such nanoperiodic assembling of semicrystalline polymers, which may play a similar role in the segmental linkages of block copolymers in terms of its transmission of the applied stress and location at the boundary between harder and softer phases. The obtained structure is applicable as a template material for the nanoporous membranes having the superior flexibility when the amorphous phases are selectively etched.

Acknowledgment. This work was partly supported by the Mitsubishi Chemical Research Foundation. SAXS measurements using synchrotron radiation were performed at the BL40B2 in the SPring-8 with the approval of the Japan Synchrotron Radiation Research Institute (JASRI) (Proposal No. 2003B0418-NL2b-np).

References and Notes

(1) Lee, J.-S.; Hirao, A.; Nakahama, S. *Macromolecules* **1989**, *22*, 2602.
(2) Hashimoto, T.; Tsutsumi, K.; Funaki, Y. *Langmuir* **1997**, *13*, 6869.
(3) Zhao, D.; Yang, P.; Melosh, N.; Feng, J.; Chmeika, B. F.; Stucky, G. D. *Adv. Mater.* **1998**, *10*, 1380.
(4) Chan, V. Z.-H.; Hoffman, J.; Lee, V. Y.; Iatrou, H.; Avgeropoulos, A.; Hadjichristidis, N.; Miller, R. D.; Thomas, E. L. *Science* **1999**, *286*, 1716.
(5) Liu, G.; Ding, J.; Stewart, S. *Angew. Chem., Int. Ed.* **1999**, *38*, 835.
(6) Jeong, U.; Kim, H.-C.; Rodriguez, R. L.; Tsai, I. Y.; Stafford, C. M.; Kim, J. K.; Hawker, C. J.; Russell, T. P. *Adv. Mater.* **2002**, *14*, 274.
(7) Ndoni, S.; Vigild, M. E.; Berg, R. H. *J. Am. Chem. Soc.* **2003**, *125*, 13366.
(8) Park, C.; Yoon, J.; Thomas, E. L. *Polymer* **2003**, *44*, 6725.
(9) Pai, R. A.; Humayun, R.; Schulberg, M. T.; Sengupta, A.; Sun, J.-N.; Watkins, J. J. *Science* **2004**, *303*, 507.
(10) Li, L.; Yokoyama, H.; Nemoto, T.; Sugiyama, K. *Adv. Mater.* **2004**, *16*, 1226.
(11) Yokoyama, H.; Li, L.; Nemoto, T.; Sugiyama, K. *Adv. Mater.* **2004**, *16*, 1542.
(12) Olayo-Valles, R.; Guo, S.; Lund, M. S.; Leighton, C.; Hillmyer, M. A. *Macromolecules* **2005**, *38*, 10101.
(13) Yokoyama, H.; Sugiyama, K. *Macromolecules* **2005**, *38*, 10516.
(14) Malik, S.; Roizrd, D.; Guenet, J.-M. *Macromolecules* **2006**, *39*, 5957.
(15) Uehara, T.; Yoshida, T.; Kakiage, M.; Yamanobe, T.; Komoto, T.; Nomura, K.; Nakajima, K.; Matsuda, M. *Macromolecules* **2006**, *39*, 3971.
(16) Uehara, H.; Yamanobe, T.; Komoto, T. *Macromolecules* **2000**, *33*, 4861.
(17) Graessley, W. W. *Adv. Polym. Sci.* **1974**, *16*, 1.
(18) Rastogi, S.; Lippits, D. R.; Peters, G. W. M.; Graf, R.; Yao, Y.; Spiess, H. W. *Nat. Mater.* **2005**, *4*, 635.
(19) Lippits, D. R.; Rastogi, S.; Hohne, G. W. H.; Mezari, B.; Magusin, P. C. M. M. *Macromolecules* **2007**, *40*, 1004.
(20) Polis, D. L.; Winey, K. I. *Macromolecules* **1996**, *29*, 8180.
(21) Polis, D. L.; Winey, K. I. *Macromolecules* **1998**, *31*, 3617.
(22) Polis, D. L.; Smith, S. D.; Terrill, N. J.; Ryan, A. J.; Morse, D. C.; Winey, K. I. *Macromolecules* **1999**, *32*, 4668.
(23) Qiao, L.; Winey, K. I. *Macromolecules* **2000**, *32*, 851.
(24) Honeker, C. C.; Thomas, E. L. *Macromolecules* **2000**, *33*, 9407.
(25) Cohen, Y.; Albalak, R. J.; Dair, B. J.; Capel, M. S.; Thomas, E. L. *Macromolecules* **2000**, *33*, 6502.
(26) Hermel, T. J.; Hahn, S. F.; Chaffin, K. A.; Gerberich, W. W.; Bates, F. S. *Macromolecules* **2003**, *36*, 2190.
(27) Shimamura, K.; Murakami, S.; Katayama, K. *Macromol. Rapid Commun.* **1982**, *3*, 199.
(28) Brady, J. M.; Thomas, E. L. *J. Mater. Sci.* **1989**, *24*, 3311.
(29) Zhou, H.; Wilkers, G. L. *Macromolecules* **1997**, *30*, 2412.
(30) Bailey, T. S.; Pham, H. D.; Bates, F. S. *Macromolecules* **2001**, *34*, 6994.
(31) Sakurai, S.; Aida, S.; Okamoto, S.; Ono, T.; Imaizumi, K.; Nomura, S. *Macromolecules* **2001**, *34*, 3672.
(32) Sakurai, S.; Aida, S.; Okamoto, S.; Sakurai, K.; Nomura, S. *Macromolecules* **2003**, *36*, 1930.
(33) Sasanuma, Y.; Law, R. V.; Kobayashi, Y.; Sasaki, K. *Anal. Chem.* **1997**, *69*, 794.
(34) Butler, M. F.; Donald, A. M. *Macromolecules* **1998**, *31*, 6234.
(35) Men, Y.; Rieger, J.; Lindner, P.; Enderle, H.-F.; Lilge, D.; Kristen, M. O.; Mihan, S.; Jiang, S. *J. Phys. Chem. B* **2005**, *109*, 16650.
(36) Uehara, H.; Matsuda, H.; Aoike, T.; Yamanobe, T.; Komoto, T. *Polymer* **2001**, *42*, 5893.
(37) Matsuda, H.; Aoike, T.; Uehara, H.; Yamanobe, T.; Komoto, T. *Polymer* **2001**, *42*, 5013.
(38) Rastogi, S.; Spoelstra, A. B.; Goossens, J. G. P.; Lemstra, P. J. *Macromolecules* **1997**, *30*, 7880.
(39) Kanamoto, T.; Tsuruta, A.; Tanaka, K.; Takeda, M.; Porter, R. S. *Macromolecules* **1988**, *21*, 470.
(40) Luo, C.; Atvars, T. D. Z.; Meakin, P.; Hill, A. J.; Weiss, R. G. *J. Am. Chem. Soc.* **2003**, *125*, 11879.
(41) Sadler, D. M.; Barham, P. J. *Polymer* **1990**, *31*, 36.
(42) Hsiao, B. S.; Yang, L.; Somani, R. H.; Avila-Orta, C. A.; Zhu, L. *Phys. Rev. Lett.* **2005**, *94*, 117802.

(43) Uehara, H.; Nakae, M.; Kanamoto, T.; Zachariades, A. E.; Porter, R. S. *Macromolecules* **1999**, *32*, 2761.
(44) Nakae, M.; Uehara, H.; Kanamoto, T.; Ohama, T.; Porter, R. S. *J. Polym. Sci., Polym. Phys. Ed.* **1999**, *37*, 1921.
(45) Nakae, M.; Uehara, H.; Kanamoto, T.; Zachariades, A. E.; Porter, R. S. *Macromolecules* **2000**, *33*, 2632.
(46) Uehara, H.; Yoshida, R.; Kakiage, M.; Yamanobe, T.; Komoto, T. *Ind. Eng. Chem. Res.* **2006**, *45*, 7801.
(47) Odell, J. A.; Grubb, D. T.; Keller, A. *Polymer* **1978**, *19*, 617.
(48) Samon, J. M.; Schultz, J. M.; Seifert, S.; Stribeck, N.; Gurke, I.; Collins, G.; Saw, C. *Macromolecules* **1999**, *32*, 8121.
(49) Schultz, J. M.; Hsiao, B. S.; Samon, J. M. *Polymer* **2000**, *41*, 8887.
(50) Keum, J. K.; Somani, R. H.; Zuo, F.; Burger, C.; Sics, I.; Hsiao, B. S.; Chen, H.; Kolb, R.; Lue, C.-T. *Macromolecules* **2005**, *38*, 5128.

MA070915Z